Transient Heating Study of Microhotplates by Using a High-Speed Thermal Imaging System

M. Afridi, D. Berning, A. Hefner, J. Suehle, M. Zaghloul, E. Kelley, Z. Parrilla, C. Ellenwood

National Institute of Standards and Technology*
Semiconductor Electronics Division
Gaithersburg, MD 20899-8124

Abstract

A high-speed thermal imaging system is used to investigate the dynamic thermal behavior of MEMS (MicroElectroMechanical Systems) based microhotplate devices. These devices are suspended microstructures fabricated in CMOS technology and are used in various sensor applications. Measurements reveal delayed surface heating of the microhotplate and temperature redistribution during both the heating and cooling phases. Reflected infrared (IR) radiation from the hidden backside of the heater is used with a normalization technique to determine peak heater temperature. The measurements are shown to be useful in optimizing the design of microhotplate structures. It is found that the use of a heat-spreading layer improves the local temperature uniformity between the heater strips. It is also found that the use of the thinner layers of the 1.5 μm CMOS technology improve the global temperature uniformity over the top surface of the microhotplate.

I. Introduction

The microhotplate has become an important component for MEMS (MicroElectroMechanical Systems) based devices and can be used for sensing elements [1] or as microscopic infrared sources [2]. Knowledge of the dynamic thermal characteristics is important for optimization of these MEMS-based devices. However, the small size and fast heating speed of microhotplate devices has made measurement of the dynamic temperature distribution difficult. The recently developed high-speed transient thermal imaging system [3] provides the only known method of measuring the transient thermal properties of this important new class of devices.

Microhotplate devices have been fabricated in silicon for some years now. One important application for such devices is the integrated gas sensor. Early examples of such devices were fabricated as discrete structures [1]. Later microhotplate fabrication used commercial CMOS processing with post-processing techniques to form the suspended membranes [4,5]. The CMOS-compatible process realizes a class of devices that are based on thermo-electro-mechanical effects and are compatible with existing VLSI circuit design techniques [6–8]. More recent work has combined the microhotplate structure with the integration of a fully functional CMOS circuit [9].

In the application of the microhotplate to practical system design, it is desirable to minimize power dissipation by using the microhotplate in pulsed-mode operation. Furthermore, pulsed mode operation can provide enhanced gas sensing in some gas-detection applications [10]. In this work, a recently developed transient thermal imaging system is used to study the dynamics of the heating and cooling phases of the microhotplate structure. It is shown for the first time that the transient thermal imaging system can be used to optimize the design of microhotplate structures and that different IC fabrication processes result in different hotplate dynamic thermal performance.

II. Test System Description

The high-speed transient thermal imaging system uses a spatial sampling and temporal averaging technique to construct a movie of a high-speed thermal event. This new system has a 15 μm spatial resolution and a 1 μs temporal resolution [3]. The system works by successively acquiring the temperature response as a function of time at each coordinate of the device under test (DUT) and by using a XY-coordinate translation stage to step between coordinates. The thermal responses at different points on the DUT are reconstructed to obtain the thermal contour movie.

Figure 1 shows the equipment used for the new measurement system. A Barnes* Engineering Computherm III infrared microscope that uses a large area InSb detector sensitive in the 1.8 μm to 5.5 μm band is used in the high-speed transient thermal imaging system. The infrared microscope is operated in "stare" mode, whereby the normal scanning mode is disabled. A Tektronix TDS 754D digitizing
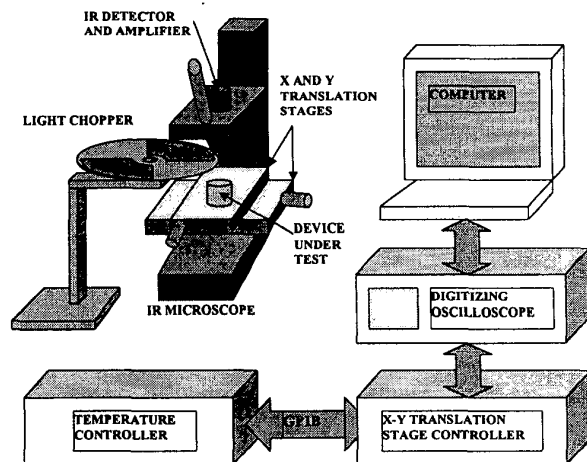

Fig. 1. Major components of the high-speed thermal imaging system.

oscilloscope is used for data acquisition, including the infrared radiation detector-amplifier output, and other DUT stimulus and response waveforms. A JC Systems temperature controller is used to maintain the DUT at a desired temperature and to facilitate emissivity calibration. A Newport MM3000 XY-coordinate motion controller is used for XY translation of the DUT under the microscope. A light chopper is used for emissivity calibration.

A sophisticated computer instrument control and high-level user interface is required for the high-speed thermal image measurements. LabWindows/CVI®⁺ virtual instrument development software is used to develop the interactive graphical computer user interface that controls instruments through the IEEE 488 instrumentation bus. This interface is used to facilitate the many instrument control functions such as data acquisition, stage translation, temperature control, and emissivity calibration. Figure 2 shows the user interface front panel for the high-speed thermal imaging system. The panel

consists of various pull down menus, buttons, and data entry/display fields used to operate the measurement system. There is an additional sub panel that is used for emissivity calibration [3], and the results of the emissivity calibration are required before accurate temperature measurements can be made via the main interface panel.

The temperature contour map on the right-hand side of the user interface panel shows the temperature distribution for a particular point in time of a transient thermal event, and the graph on the left-hand side shows the temperature response for a particular position on the DUT. The asterisk on the temperature response graph indicates the point in time for the thermal contour map, and the position on the device under test for the temperature response is indicated by the cross-hair cursor on the thermal contour map. The cursor can be moved to display the temperature response at any location on the contour map. The point in time can be changed using the frame buttons in the oval region, or the entire movie can be
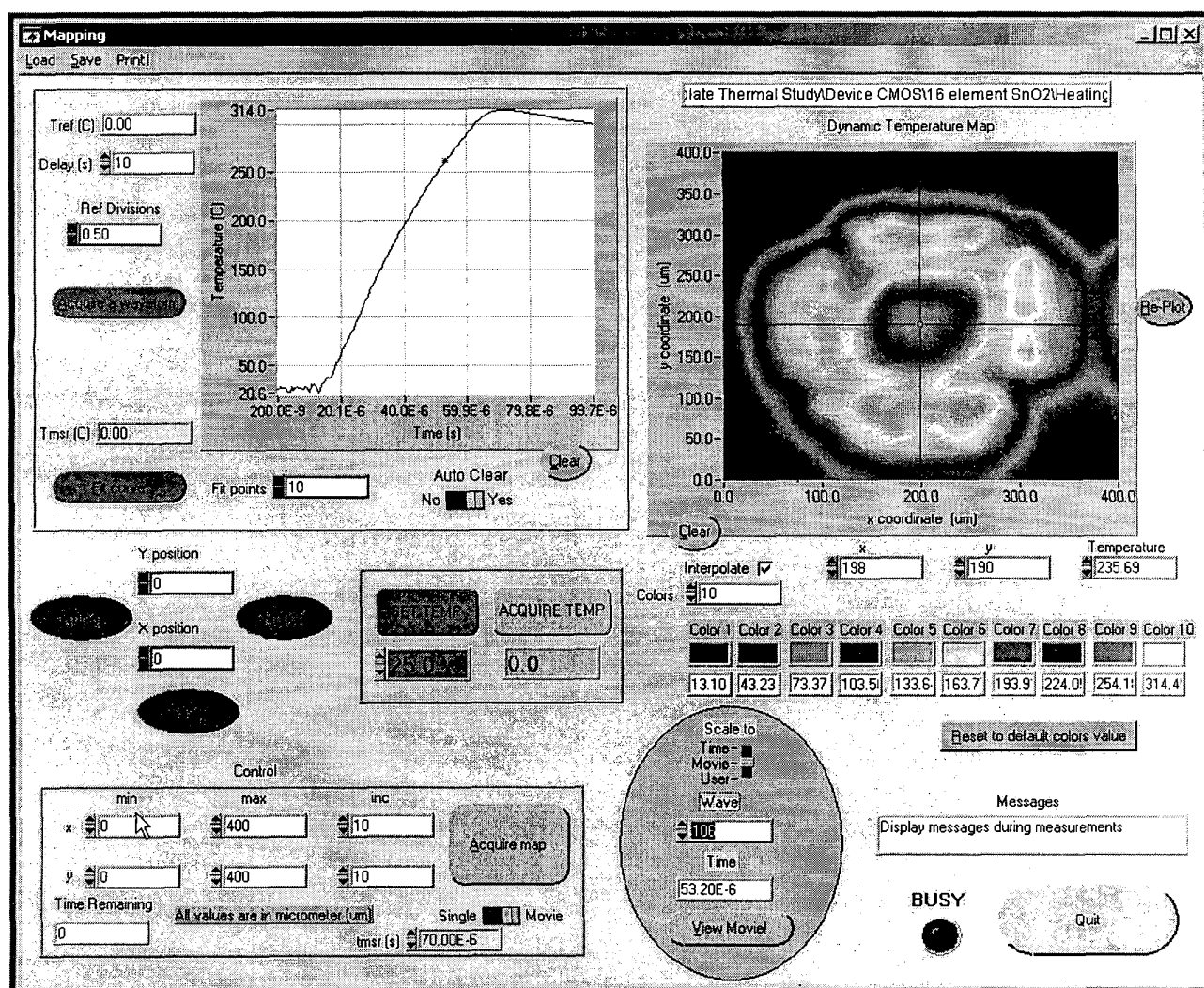

Fig. 2. Virtual instrument user interface front panel for the high-speed thermal imaging system.

and Technology, nor does it imply that the products are the best for the purpose.

⁺ LabWindows/CVI® is a trademark of National Instruments Inc.

viewed using the "view movie" button.

III. MICROHOTPLATE STRUCTURE

To study the design parameters influencing the thermal performance of microhotplates and gas sensors, devices were fabricated using three different CMOS technologies, two different post process etching techniques, different size heater elements, and different device designs.

The microhotplates studied in this work are fabricated using CMOS microfabrication technology normally used for manufacturing integrated circuits. Post-processing steps are then used to remove silicon beneath fabricated layers, forming a suspended membrane. Additional post-processing steps can be used to deposit films on top of the membrane to form the gas-sensing element. The conductivity of the sensing film (e.g., SnO_2) at high temperatures (100 °C to 450 °C) is sensitive to the presence of specific gases. Suspended structures are required to achieve high thermal efficiency in this temperature range.
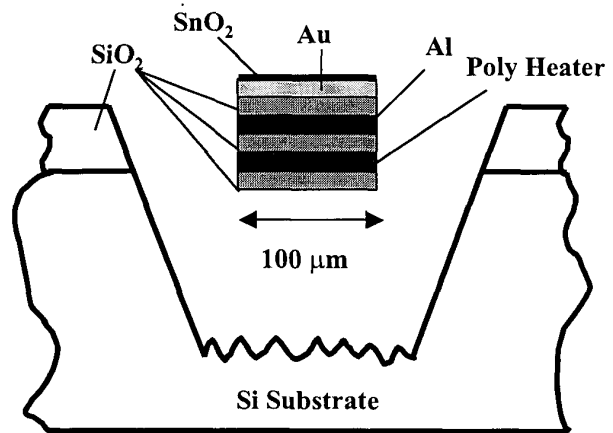
The CMOS foundry microfabrication processes provide multiple layers of different materials needed to form semiconductor devices and interconnections for integrated circuits. The design layout file defines the material layers present in each region of the integrated circuit. Using this file, both microhotplates and accompanying electronic circuits can be implemented on the same substrate.

Figure 3 shows (a) the layer components of the membrane that is suspended after the post processing etch and (b) an SEM micrograph of the suspended membrane for the 2 μm CMOS-based microhotplate. The SiO_2 layers are used by the CMOS process to provide isolation between interconnect layers and to form gate insulators for the MOSFET devices. For the microhotplate devices, the SiO_2 layers are used to provide isolation between the heating, sensing, and heat spreading layers and to provide strength to the suspended membrane. The polysilicon layer used to form the MOSFET transistor gates and resistors for integrated circuits is used as the heating element in the microhotplate. The aluminum layer used for interconnection between transistors in integrated circuits is used as a heat spreader in the microhotplate. The gold and the tin-oxide layers are post-processed, application-specific layers used for a gas-sensing application.
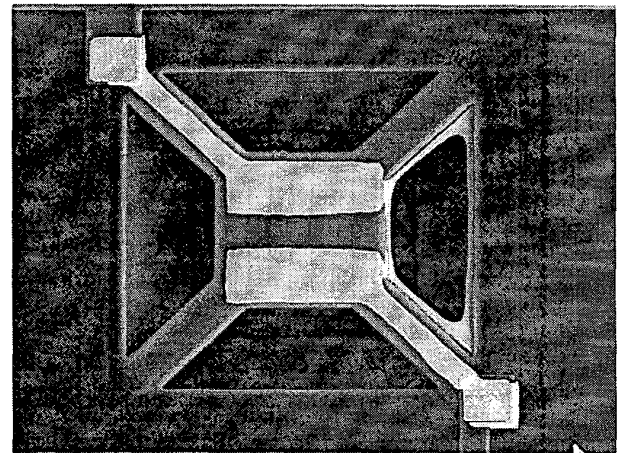
IV. MICROHOTPLATE TRANSIENT THERMAL RESULTS

In this section, transient heating and cooling results are given for several different microhotplate designs. These devices are fabricated using three different processes; a standard 2 μm CMOS technology, a standard 1.5 μm CMOS technology, and a full custom microfabrication process. The different processes incorporate different materials and thickness for the layers shown in Fig. 3(a). Suspended membranes of different sizes are studied in this work, although only results of the 100 μm by 100 μm devices are presented. Devices with and without a heat spreader are studied for the case of the full custom process.

To perform the transient thermal measurements, a repetitive low duty-cycle voltage stimulus is applied to the microhotplate-heating element. The tests range form high-amplitude narrow heating pulse widths to low-amplitude wide heating pulse widths. These different heating pulse widths are

(a)

(b)

Fig. 3. Microhotplate – (a) Cross section of layer structure; (b) SEM micrograph of the suspended structure prior to SnO_2 deposition.

used to study various thermal time constants associated with the microhotplates. The higher voltages amplitude is used for the narrower heating pulse widths so that the device reaches its intended operating temperature point during the pulse. The transient heating and cooling results for the different microhotplate device technologies are discussed separately below.

A. 2 μm CMOS-Based Microhotplate

Transient thermal measurements are performed using voltage pulse widths ranging from 10 μs to 10 ms to determine the thermal time constants of various portions of the microhotplate structure. It is determined that this structure reaches steady state after about 10 ms for long heating pulses and also requires about 10 ms for cooling.

Figure 4 shows a sequence of thermal images for a 48 μs heating pulse where the pulse begins at the 12 μs point and terminates at the 60 μs point. The point in time during the pulse is indicated by the asterisk on the microhotplate center-point temperature response waveform to the left of each image. The thermal contour values and colors are defined at
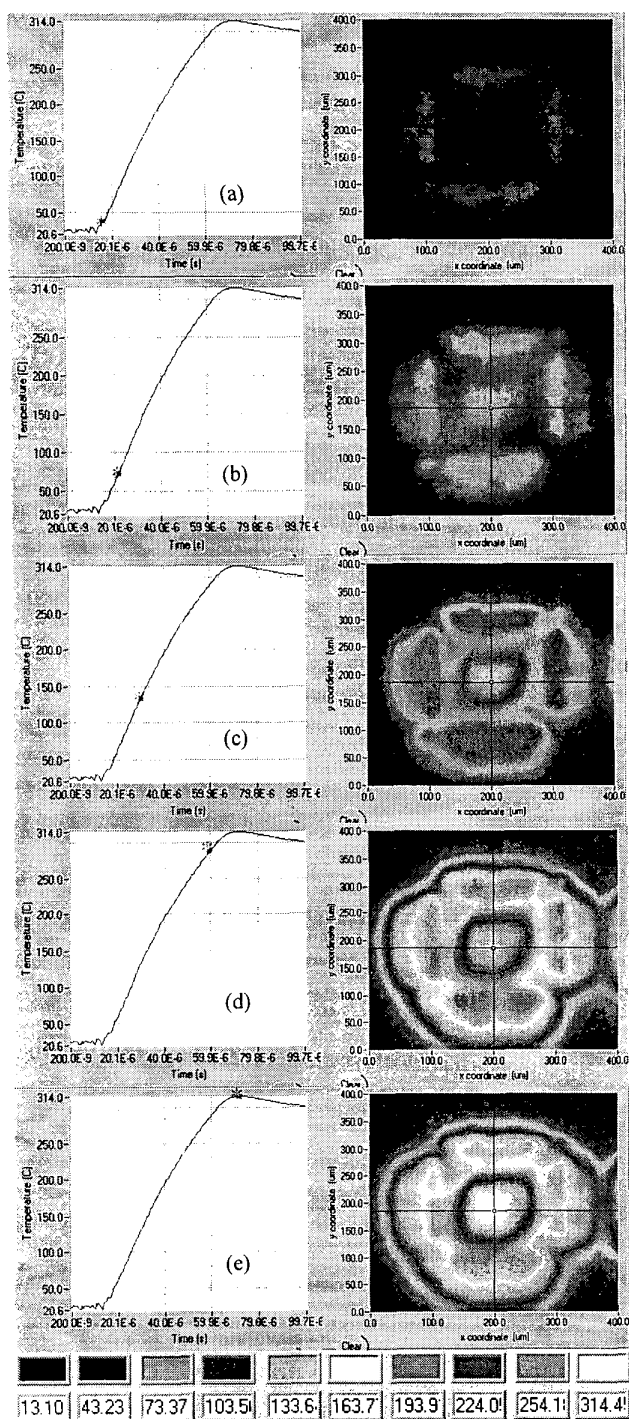
Fig. 4. Sequence of thermal images during rapid heating of the microhotplate structure where each thermal contour map (right) corresponds to a point in time shown by the asterisk on the associated center point temperature waveform (left). The thermal contour values and colors are defined at the bottom of the figure. In (a), heating has just begun, and only reflected radiation emitted from the window area is observed. Heating progresses with (b-d), and power is removed at (d). The temperature of the top surface reaches its maximum in (e), 12 μs after power is removed form the heating element at the bottom surface of the suspended membrane.

the bottom of the figure in degrees Celsius. For these measurements, an 80 V rectangular voltage pulse is applied to the heating element, resulting in a 3.2 W pulsed heating condition. The polysilicon heating elements used in this study have resistances that range from 2 kΩ to 4 kΩ.

When power is applied to the heater, the temperature of the heating element on the bottom surface of the suspended membrane begins to increase, whereas there is a delay in temperature rise for the top surface due to the thermal isolation of the SiO_2 layers. The heat from the bottom surface of the membrane is observed through the windows around the suspended structure (Fig. 4(a)) due to infrared radiation that is emitted from the bottom surface of the membrane and reflected off of the bottom of the silicon etched pit. The temperature of the bottom surface of the microhotplate can be determined using the normalization technique described later in this section.

The temperature of the top surface of the membrane rises (Figs. 4(b) and 4(e)) as the heat is conducted from the heating element at the bottom surface of the membrane through the oxide layers that electrically insulates the heater from the sensing film and through the aluminum heat spreader. Power to the heater is terminated at the 60 μs point (Fig. 4(d)), whereas the temperature of the top surface has not reached its maximum as indicated by the rise after the asterisk on the graph of Fig. 4(d). In Fig. 4(e) the temperature of the top surface reaches its maximum about 12 μs after the power is terminated. In Fig. 4(e), it is clear that the IR radiation emitted from the window area is reduced, indicating that the temperature of the bottom surface of the suspended membrane has fallen while the temperature of the top surface has risen.

Figure 5 shows the microhotplate transient temperature response to a fast 10 μs heating pulse both at the center of the suspended heater and 10 μm off center. The time required for the surface temperature to equalize after the heating pulse is removed (35 μs in Fig. 5(a)) represents the membrane lateral redistribution thermal time constant that is influenced by the aluminum heat spreader. Figure 5(b) shows the influences of both the 35 μs membrane lateral time constant and the time required for the entire membrane to cool (10 ms). The membrane cooling time is determined by the total heat capacity of the suspended membrane and heat removal due to radiation, convection, and thermal conductance through the membrane-supporting legs.

The underside of the suspended membrane reaches a higher peak temperature under transient conditions relative to the top surface. This is because the polysilicon heater is near the bottom of the suspended membrane structure and the structure has thermally insulating SiO_2 layers between the heater and the metal layers on the top surface (see Fig. 3). It is important to know the peak temperature of the polysilicon heater for reliability reasons; however only the temperature of the top surface can be measured directly. The peak temperature of the underside of the structure can be determined by comparing transient heating responses of the reflected IR radiation emitted from the window area with the responses obtained from the top surface. Since only a fraction of the bottom surface radiation is reflected through the
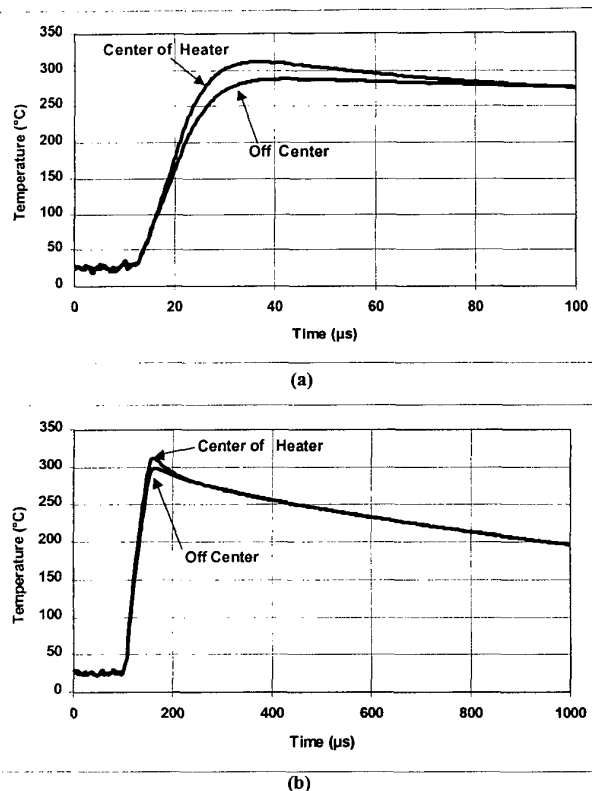
95   18th IEEE SEMI-THERM Symposium

Fig. 5. The 2 µm CMOS-based microhotplate transient temperature response to a 10 µs heating pulse. The waveforms represent measurements at the center of the heater and off center, and show (a) a 35 µs membrane lateral redistribution time constant; and (b) long term membrane cooling.
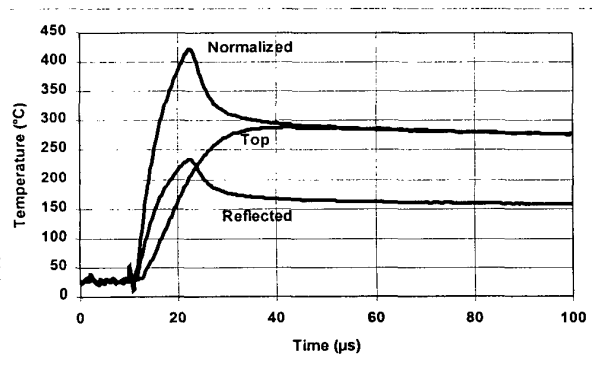

Fig. 6. The top, reflected, and normalized transient temperature response for the 2 µm CMOS-based microhotplate demonstrating normalization technique of measuring temperature of the hidden underside of the microhotplate.

windows, a normalization technique can be used to determine the peak temperature of the bottom surface.

Figure 6 shows how normalization is used to predict the peak temperature of the underside of the microhotplate for a 10 µs heating pulse that begins at the 13 µs point and ends at the 23 µs point. The response labeled "reflected" is from the
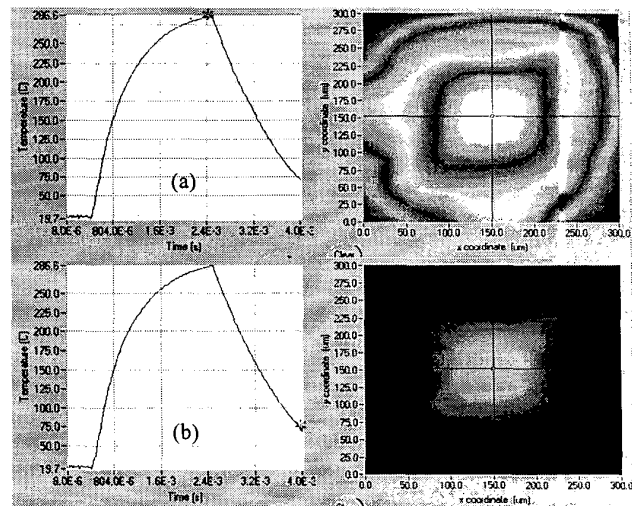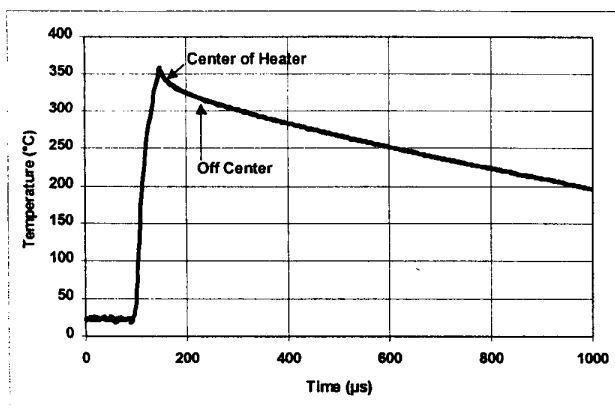

Fig. 7. Thermal images of 1.5 µm CMOS-based microhotplate (a) at maximum temperature and (b) after partially cooled.

IR radiation captured through the window area, and the response labeled "top" is the measured top surface temperature. The response labeled "normalized" is obtained by multiplying the "reflected" response by a constant reflection coefficient. This normalization is possible because the temperature of the top and bottom surfaces of the microhotplate become equalized rapidly after the power is removed due to the conduction through the thin oxide layers. As a result, the measured response of the bottom surface can be aligned with the measured temperature of the top surface after the short 10 µs redistribution time constant. The peak temperature obtained from the normalized response is about 425 °C. From these temperature responses, it can be seen that the top sensing-film temperature crosses the 200 °C level 10 µs later than the bottom surface. The bottom surface of the microhotplate reaches its peak temperature when the power is turned off (23 µs point in Fig. 6), whereas the top surface reaches its maximum temperature much later (40 µs point).
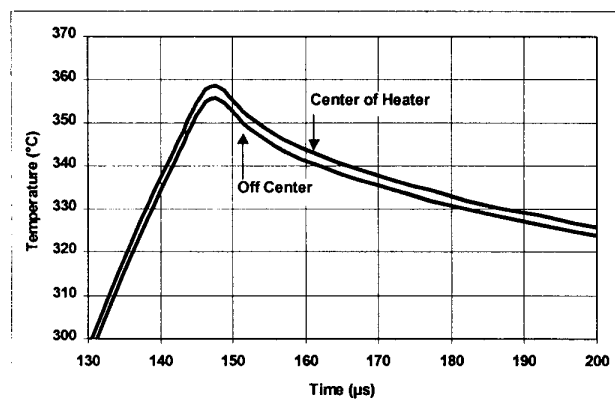
B. 1.5 µm CMOS-Based Microhotplate

Figure 7 shows thermal images with associated heating and cooling responses for the 1.5 µm CMOS-based microhotplate. A relatively long (2 ms) heating pulse is used, and the microhotplate temperature is approaching steady state before the heating pulse is removed. In Fig. 7(a), a temperature contour map is shown for the maximum temperature point, and in Fig. 7(b) a map is shown for 1.5 ms after power is removed and the microhotplate has substantially cooled. In the image associated with Fig. 7(b), the four suspending legs for the microhotplate retain a small amount of heat and are visible.

Figure 8 shows the microhotplate transient temperature response to a short 10 µs heating pulse both at the center of the structure and approximately 10 µm off center. Fig. 8(b) shows an expanded view of the peak temperature region of the temperature response shown in Fig. 8(a). For the 1.5 µm CMOS-based microhotplate, there is almost no difference in
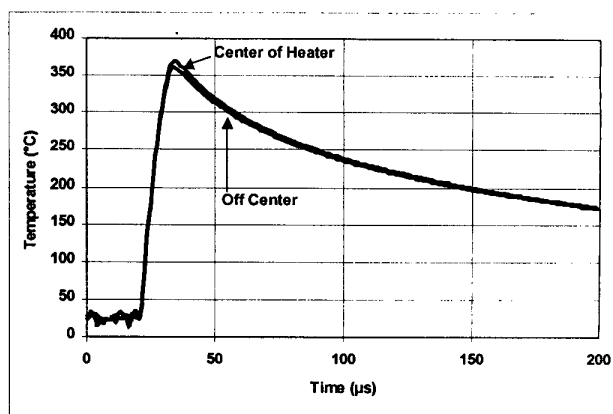
96   18th IEEE SEMI-THERM Symposium

Fig. 8. The 1.5 μm CMOS-based microhotplate transient temperature response to a 10 μs heating pulse. The waveforms represent measurements at the center of the heater and off center, and show (a) uniform temperature distribution and (b) expanded view of the peak temperature region.

Fig. 9. Transient temperature responses of the custom microhotplate with a heat spreader to a 10 μs heating pulse both at the center of the heater and off center. These temperature waveforms show (a) minor transient temperature differences and (b) a 10 °C maximum temperature difference near the peak temperature region.
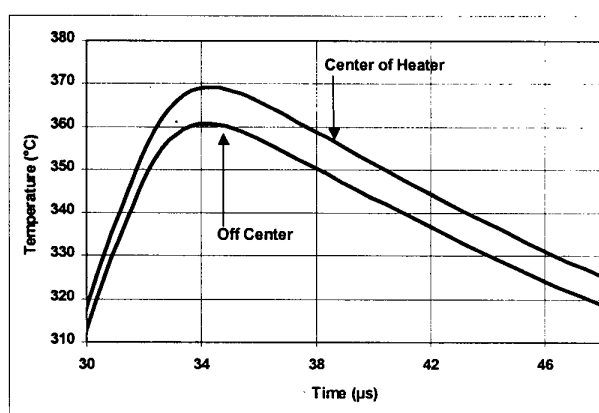
the shape and only a small shift in temperature between the center and off center responses. This can be compared to the results for the 2 μm CMOS-based microhotplate shown in figs. 5(a) and 5(b) where there is a significant difference in the response shapes on and off center. Apparently, the thinner layers of the 1.5 μm CMOS technology process improve the temperature uniformity and effectively eliminate the time constant associated with lateral heat redistribution on the top surface of the microhotplate.

C. Custom Process-Based Microhotplate

Figure 9 shows microhotplate transient temperature responses for devices made using a full custom process. This device incorporates a heat-spreading layer similarly to the devices described above. The temperature response curves are for a 10 μs heating pulse both at the center of the structure and about 10 μm off center. The shapes of the responses on and off center are similar and show smooth temperature decay once power is removed. It can be seen from the expanded view of Fig. 9(b) that the peak temperature difference between the center and off center is approximately 10 °C.

Figure 10 shows the transient temperature responses of a similar device made in the custom process but without a heat-spreading layer. The temperature response curves are for a 10 μs heating pulse both at the center of the structure and about 10 μm off center. Fig. 10(b) shows that the peak temperature difference between center and off center is also about 10 °C for the device without the heat spreader. Although the temperature responses are similar for both the on-center and off-center positions of this second device, there are significant differences in the measured cooling responses between devices with and without a heat spreader.

In the case of the microhotplate without the heat spreader, there is an initial rapid fall in temperature with a very short thermal time constant followed by the slowly decaying portion that is similar to the device with the heat spreader. The rapid initial fall in temperature for the device without the heat spreader is caused by the rapid redistribution of heat from the polysilicon heater strips to the spaces in between the heater strips once the power is removed as described below. These results indicate that the heat spreader is effective in eliminating local variations in dynamic temperature distribution.
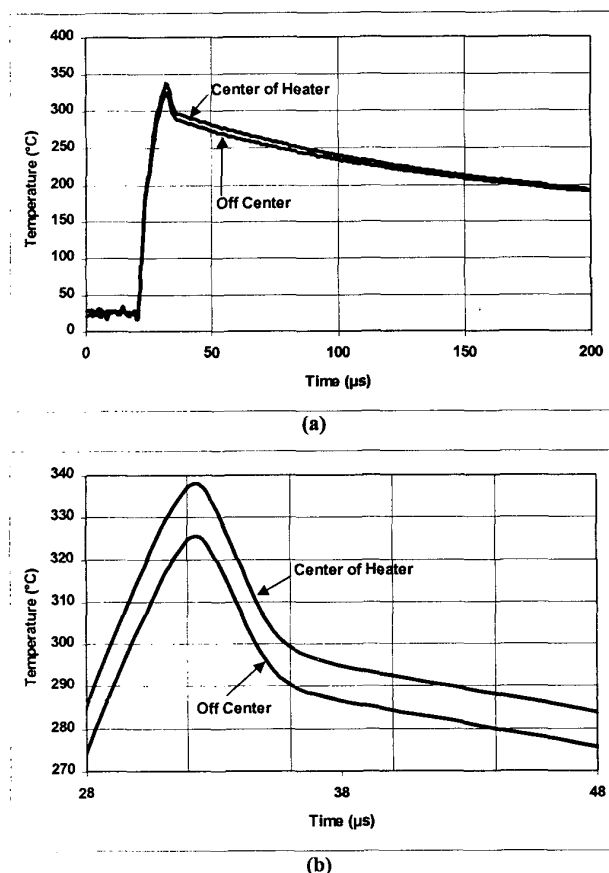
18th IEEE SEMI-THERM Symposium

Fig. 10. Transient temperature responses of the custom microhotplate without a heat spreader to a 10 μs heating pulse both at the center of the heater and off center, indicating a rapid initial temperature decay once power is removed. (a) Long term and (b) magnified near the peak temperature region.

The microhotplate structures consist of heater stripes that are 10 μm wide and separated by 3 μm spaces. These dimensions are too fine to be resolved spatially by the IR detector, which is limited to 15 μm spatial resolution. Since the output of the IR detector is nonlinear and approximately follows a polynomial of seventh degree, the measured temperature is highly weighted toward the peak temperature within the 15 μm focal area. The rapid initial decay of temperature shown in Fig. 10 is caused by the reduction in peak temperature at the center of the heater stripes as the heat redistributes to region between the stripes.

IV. CONCLUSION

In this paper, a high-speed thermal imaging system is used to study the transient thermal characteristics of microhotplate structures. It is shown that the unique high-speed thermal imaging system is capable of determining various thermal time constants of the structure. These time constants include the propagation of heat from the heating element through the multi-layered suspended membrane structure, the equalization of temperature over the top surface, and the cooling of the entire membrane structure by convection, radiation, and conduction through the legs. It is also shown that reflected IR radiation can be used with a normalization technique to determine the temperature of the hidden underside of the suspended membrane. The thermal time constants measured with the transient thermal imaging system can be used to optimize the thermal performance of microhotplates. These measurement results show the importance of the microhotplate heat-spreading layer in obtaining a uniform dynamic temperature distribution.

REFERENCES

[1] V. Demarne and A. Grisel, "An Integrated Low-Power Thin-Film CO Gas Sensor on Silicon," Sensors and Actuators, vol. 13, pp. 301-313, 1988.

[2] M. Parameswaran, A. M. Robinson, D. L. Blackburn, M. Gaitan, and J. Geist, "Micromachined Thermal Radiation Emitter from a Commercial CMOS Process," IEEE Electron Device Lett., vol. 12, no. 2, pp. 57-59, Feb. 1991.

[3] A. Hefner, D. Berning, D. Blackburn, C. Chapuy, and S. Bouche, "A High-Speed Thermal Imaging System For Semiconductor Device Analysis," Conference Proceedings Seventeenth Annual IEEE Semiconductor Thermal Measurement and Management Symposium, pp. 43-49, March 2001.

[4] M. Parameswaran, H. P. Baltes, Lj. Ristic, A. C. Dhaded, and A. M. Robinson, "A New Approach for the Fabrication of Micromachined Structures," Sensors and Actuators, vol. 19, pp. 289-307, 1989.

[5] J. S. Suehle, R. E. Cavicchi, M. Gaitan, and S. Semancik, "Tin Oxide Gas Sensor Fabricated Using CMOS Micro-Hotplates and In-Situ Processing," IEEE Electron Device Letters, vol. 14, no. 3, p. 118, March 1993.

[6] M. Parameswaran, A. M. Robinson, Lj. Ristic, K. Chau, and W. Allegretto, "A CMOS Thermally Isolated Gas Flow Sensor," Sensors and Materials, vol. 2, pp. 17-26, 1990.

[7] D. Moser, O. Brand, and H. Baltes, "A CMOS Compatible Thermally Excited Silicon Oxide Beam Resonator with Aluminum Mirror," in Proc. Transducers '91, pp. 547-550, 1991.

[8] J. Jaeggi, H. Baltes, and D. Moser, "Thermoelectric AC Power Sensor by CMOS Technology," IEEE Electron Device Lett., vol. 13, no. 7, p. 366, 1992.

[9] M Afridi, J. Suehle, M. Zaghloul, J. Tiffany, R. Cavicchi, "Implementation of CMOS Compatible Conductance-Based Micro-Gas-Sensor System," European Conference on Circuit Theory and Design, pp. (III) 381-384, August 2001.

[10] R. E. Cavicchi, J. S. Suehle, K. G. Kreider, M. Gaitan, and P. Chaparala, "Fast Temperature Programmed Sensing for Micro-Hotplate Gas Sensors," IEEE Electron Device Letters, 16, pp. 286-288, 1995.